Title
Utility of spatial frequency domain imaging (SFDI) and laser speckle imaging (LSI) to non-invasively diagnose burn depth in a porcine model

Journal
Burns, 41(6)

ISSN
0305-4179

Authors
Burmeister, David M
Ponticorvo, Adrien
Yang, Bruce
et al.

Publication Date
2015-09-01

DOI
10.1016/j.burns.2015.03.001

HHS Public Access

Author manuscript

Burns. Author manuscript; available in PMC 2016 September 01.

Published in final edited form as:

Burns. 2015 September ; 41(6): 1242–1252. doi:10.1016/j.burns.2015.03.001.

Utility of spatial frequency domain imaging (SFDI) and laser speckle imaging (LSI) to non-invasively diagnose burn depth in a porcine model☆

David M. Burmeister[a,1], **Adrien Ponticorvo**[b,1], **Bruce Yang**[b], **Sandra C. Becerra**[a], **Bernard Choi**[b,c], **Anthony J. Durkin**[c], and **Robert J. Christy**[a,*]

[a]United States Army Institute of Surgical Research, 3698 Chambers Pass, JBSA Fort Sam Houston, TX 78234, USA

[b]Beckman Laser Institute and Medical Clinic, University of California Irvine, 1002 Health Sciences Road East, Irvine, CA 92617, USA

[c]Biomedical Engineering Department, University of California Irvine, 3120 Natural Sciences II, Irvine, CA 92697, USA

Abstract

Surgical intervention of second degree burns is often delayed because of the difficulty in visual diagnosis, which increases the risk of scarring and infection. Non-invasive metrics have shown promise in accurately assessing burn depth. Here, we examine the use of spatial frequency domain imaging (SFDI) and laser speckle imaging (LSI) for predicting burn depth. Contact burn wounds of increasing severity were created on the dorsum of a Yorkshire pig, and wounds were imaged with SFDI/LSI starting immediately after-burn and then daily for the next 4 days. In addition, on each day the burn wounds were biopsied for histological analysis of burn depth, defined by collagen coagulation, apoptosis, and adnexal/vascular necrosis. Histological results show that collagen coagulation progressed from day 0 to day 1, and then stabilized. Results of burn wound imaging using non-invasive techniques were able to produce metrics that correlate to different predictors of burn depth. Collagen coagulation and apoptosis correlated with SFDI scattering coefficient parameter (μ_s') and adnexal/vascular necrosis on the day of burn correlated with blood flow determined by LSI. Therefore, incorporation of SFDI scattering coefficient and blood flow determined by LSI may provide an algorithm for accurate assessment of the severity of burn wounds in real time.

Keywords

Burn diagnosis; Non-invasive imaging; Swine

☆The opinions or assertions contained herein are the private views of the author and are not to be construed as official or as reflecting the views of the Department of the Army or the Department of Defense.

*Corresponding author at: Extremity Trauma and Regenerative Medicine, United States Army Institute of Surgical Research, 3698 Chambers Pass, BHT1:Bldg 3611, JBSA Fort Sam Houston, TX 78234-6315, USA. Tel.: +1 210 539 9528; fax: +1 210 539 3877. Robert.j.christy12.civ@mail.mil.

[1]These authors contributed equally to this work.

Conflict of interest: We wish to confirm that there are no known conflicts of interest associated with this publication.

1. Introduction

Over a half million people seek treatment annually for burns [1]. Excision and grafting is the most common surgical procedure performed after burn, with estimates as high as 66% of all burns undergoing surgery [2,3]. Categorically, first degree burns will heal spontaneously and do not benefit from surgical intervention. Third degree burns are the most severe and benefit most from excision/debridement because they will not heal spontaneously; additionally, first and third degree burns are easily identified based on visual inspection. Intermediate of these two extremes are second degree wounds which present a diagnostic challenge using visual inspection alone. The accuracy of diagnosis of second degree burn severity has been reported to be only 60–80% and is further reduced if the diagnosis is made within the first 48 h after-burn [4–8].

The treatment strategy for second degree burns depends on the actual burn severity. Superficial second degree burns, which are similar to first degree burns, are treated conservatively (i.e. covered and monitored) and will normally heal within 1–2 weeks. Deeper second degree burns, are similar to third degree burns and benefit from debridement/escharotomy and grafting as early as possible. Early excision has been shown to reduce the occurrence of infection and wound healing complications, thus shortening the duration of hospital stays [9–11]. Therefore, inaccurate burn severity diagnosis can have drastic consequences for the patient. If burn depth is overestimated, unnecessary surgeries may be performed. If burn depth is underestimated, the increased delay in treatment time can lead to the morbidities mentioned above, and result in impaired cosmesis and function (e.g. limited range of motion) due to scar formation. Clearly, an objective and quantifiable measure that would accurately assess burn severity would improve patient outcomes.

To this end, a number of non-invasive imaging techniques have been investigated for their use in determining burn depth, including terahertz imaging, infrared spectroscopy, and reflectance mode confocal microscopy [12–17]. The most successful of these techniques implement some aspect of examining blood flow, exploiting readouts such as temperature changes or vascular patency. Perhaps the most promising of these techniques studied thus far are laser Doppler imaging (LDI) and indocyanine green angiography (ICG), however both of these have caveats to their use [5]. To perform ICG it is necessary to inject a fluorescent dye intravenously; this procedure is associated with several side effects, from mild headaches and pruritus to the potential for a severe anaphylactic response [18]. LDI has been shown to accurately assess burn severity [19], however, LDI has several limitations including long scan times, and superficial resolution. Moreover, it has been shown that LDI is only superior to visual assessment after 48 h after-burn [8].

Two emerging technologies, laser speckle imaging (LSI) and spatial frequency domain imaging (SFDI) have recently been shown to provide accurate assessments of burn depth. LSI measures blood flow, with similar consistency as LDI [20]. LSI, however, is easier, less expensive, and allows improved patient comfort than LDI. Additionally, LSI provides real time perfusion maps that allow for evaluation of blood flow in relation to the patient's anatomy. SFDI is a wide-field imaging modality that non-invasively yields quantitative

spatial maps of tissue optical properties and biochemical composition. These include concentration of chromophores, such as oxyand deoxyhemoglobin, as well as structural tissue matrix integrity via scattering coefficients (μ_s) [21–24]. Recently, SFDI has been shown to be able to predict burn severity in a rodent comb burn wound model [25].

While a variety of techniques have been employed in burn research, histopathology is still used because of its accuracy. Masson's trichrome staining is the most often used histological stain, however other immunohistochemical stains have recently been shown to be superior in determining burn depth [26–28]. Specifically, caspase 3 is a protease that is involved with the activation phase of cell apoptosis. Staining tissue early after burn wounding with caspase 3 antibodies has been shown to stain distinct bands of apoptotic cells, delineating burn depth as early as 1 day after-burn. Additionally, high mobility group box protein 1 (HMGB1) has recently been identified as being able to define the zone of stasis, identifying initially viable tissue that eventually becomes necrotic [27]. Moreover, both of these markers correlated with each other, and with the eventual level of tissue necrosis seen at 7 days [27]. Histopathology has been proposed for use clinically, but is seldom used due to the invasiveness of the procedure, which could be circumvented if other non-invasive techniques were available to measure apoptotic or necrotic cell death.

The current study was designed to examine whether LSI and/or SFDI have the ability to non-invasively measure burn depth in a porcine model. It is well accepted that porcine skin closely resembles humans in terms of structure and wound healing [29,30]. We used a contact burn procedure with brass probes to create burn wounds spanning from superficial to full thickness. The current clinical standard of histopathology was used to define burn depth using three main methods; collagen coagulation (trichrome staining), cellular apoptosis (caspase 3), and vascular/adnexal necrosis (HMGB1). The results show that LSI and SFDI are able to non-invasively predict different burn which may aid the clinician in diagnosing burn depth.

2. Materials and methods

2.1. Animals

Two female Yorkshire swine (Midwest Research Swine) weighing 49 and 50 kg at the time of burn were used in this study. Animals were singly housed, with ad libitum access to water, and were allowed to acclimate to the facilities for at least 7 days prior to any procedures. This protocol (A13-018) was approved by the Animal Care and Use Committee, Institute of Surgical Research. This study has been conducted in compliance with the Animal Welfare Act, the implementing Animal Welfare Regulations, and the principles of the Guide for the Care and Use of Laboratory Animals.

2.2. Anesthesia

Animals were fasted and a transdermal fentanyl patch (100 μg/h) was placed on the ear of the animals on the night before the procedure. The next morning (day 0), the animals were premedicated with glycopyrrolate (0.01 mg/kg, IM) to minimize salivation and bradycardia during the surgical procedure. Anesthesia was induced with an IM injection of tiletamine-zolazepam (Telazol, 6 mg/kg). The animals were then intubated with an endotracheal tube

and placed on an automatic ventilator with the initial tidal volume at 10 ml/kg, peak pressure at 20 cmH_2O and respiration rate at 8–12 breaths per minute. The ventilator setting was adjusted to maintain an end tidal PCO_2 of 40 ± 5 mmHg, and anesthesia was maintained with 1–3% isoflurane in 100% oxygen. On days 1–4 after-burn the animals were also briefly anesthetized in order to obtain SDI and LSI images and wound biopsies. For these follow-ups, animals were sedated with 10–20 mg/kg ketamine intramuscularly, and maintained under mask anesthesia (3–5% isoflurane).

2.3. Thermal injury

Prior to burning, hair was removed from the dorsum of the swine with clippers, and the back was sterilized with chlorhexidine. The creation of wounds was completed using a custom designed burn device consisting of 3 cm diameter brass probes with stainless steel posts and a Delrin® insulated handling device described previously [31]. The brass probes were placed in a hard-anodized aluminum block, and heated in a warm bath incubator to 100 °C. This Delrin® insulated portion of the handling device is spring loaded and is placed flush on the skin to ensure a consistent, reproducible pressure when probes are applied to the animals. Wounds were located 1.5 cm from the spine and 2.5 cm away from each other in order to ensure each wound would be independent and free of competing healing responses from adjacent burn areas. Eight wounds were created on both sides of the spine in both animals for a total of 32 burns. Eight contact times; 5,10,15, 20, 25, 30, 35, and 40 s were used, leading to a total of $n = 4$ per contact time. After all burn wounds were imaged, the wounds were covered with sterile non-adherent gauze (Telfa, Tyco Healthcare, Mansfield, MA), antibiotic Ioban™ dressing (3M, St. Paul, MN), which were held in place with surgical tape (Elastikon, Johnson and Johnson, New Brunswick, NJ) followed by an antibiotic occlusive dressing (Ioban™ 2, #M, St. Paul, MN).

2.4. Spatial frequency domain imaging (SFDI)

Image acquisition for the prototype SFDI system was carried out with custom C# software (v100, Modulated Imaging Inc., Irvine, CA). A description of the instrumentation has been documented previously [32,33], Briefly, the instrument contained LEDs centered at 658, 730, and 850 nm [34] that were projected off of a spatial light modulator, Digital Micromirror Device (DMD Discovery™ 1100, Texas Instruments Inc., Dallas, TX) and then collected with a near-infrared camera. The camera field of view was approximately 13.5 cm × 10.5 cm and the spatial light modulator projected a sinusoidal pattern of 0.2 mm^{-1} at three phases for each of the LEDs. It took approximately 12 s to collect one sequence of data, and this process was repeated three times. The coefficient of variation (standard deviation/mean) for SFDI-derived parameters were obtained by taking a minimum of 5 measurements on normal skin and/or a skin-mimicking static phantom over the course of the experiment.

The procedure for determining absorption and reduced scattering coefficients (μ_s') from the images of the projected patterns has also been detailed previously [25,32,33]. Reduced scattering coefficients incorporate the scattering coefficients (μ_s) and the anisotropy of the observed tissue. Using MATLAB to analyze the images (planar and modulated) for each LED, the absorption and μ_s' were estimated based on Monte Carlo simulations [35]. The

absorption maps were used to determine the concentration of oxygenated and deoxygenated hemoglobin which could be converted to tissue oxygen saturation (stO_2) by dividing oxygenated hemoglobin by the sum of oxygenated and deoxygenated hemoglobin, [22]. Regions of interest in each image were selected at the spaces where biopsies would later be taken.

2.5. Laser speckle imaging (LSI)

The LSI instrument consists of three main components: a laser source to generate the laser speckle pattern, a CCD camera to capture the image, and a computer to process the data. The laser source was a continuous-wave HeNe laser light (λ = 633 nm, 30 mW, Edmund Industrial Optics, Barrington, NJ). The CCD camera was a thermoelectrically-cooled (Retiga 2000R, QImaging, Burnaby, BC, Canada) with a pixel resolution of 1600 × 1200 (7.4 μm × 7.4 μm). The laptop (Sager NP170, City of Industry, CA) was equipped with a GTX650 Graphics Processing Unit (GPU) (NVIDIA, Santa Clara, CA) and used custom LabVIEW (Version 8.0, National Instruments, Austin, TX) software to process images at a rate of eight frames per second [36,37]. The procedure for acquiring and processing speckle images into blood flow maps within a dermatological setting have been detailed previously [36]. Briefly, a speckle pattern created by the 633 nm laser is projected over the region of interest, recorded by the camera and processed to generate a blood flow map based on a metric known as Speckle Flow Index, SFI [38]. Due to the motion sensitive nature of LSI, multiple respiratory cycles are sampled and SFI values are acquired at the trough of the respiratory cycle. The visible rectangular region seen in Fig. 2C is representative of the region used to monitor respiration, but sampled SFI regions include an area extending beyond the box. The coefficient of variation (standard deviation/mean) for LSI-derived blood flow was obtained by taking a minimum of 5 measurements on normal skin and/or a skin-mimicking static phantom over the course of the experiment.

2.6. Histological analysis

On day 4 after-burn, a strip of tissue spanning the entire wound bed (approximately 3.5 × 0.5 cm) was harvested on the transverse axis. These samples (n = 4 samples/contact time) and biopsies from the previous days (n = 4 samples/contact time/day) were fixed in 10% buffered formalin for 48 h, processed, embedded in paraffin and then cut into 6 μM cross-sectional slices. Slides were deparaffinized in xylene and rehydrated to water and stained. All samples were stained with trichrome reagents (Masson Kit, Sigma Aldrich®, St. Louis, MO).

Tissue sections for immunohistochemistry (IHC) were prepared as follows: heat-mediated antigen retrieval step was used with 0.01 M citrate buffer at 95–98 °C for 15 min; endogenous peroxidase activity was blocked with 0.3%H_2O_2 for 20 min at room temperature; non-specific IgG blocking was performed with 10% horse serum in Hanks' balanced salt solution (HBSS) for 30 min at room temperature. The tissue sections were then incubated with primary antibody diluted in 3% horse serum: caspase 3 (abcam, ab4051, rabbit polyclonal, 1:300 dilution) and HMGB1 (abcam, ab18256, rabbit polyclonal, 1:200 dilution) and incubated at room temperature for 60 min. Following primary antibody incubation, slides were treated with secondary antibody (Biotinylated Horse Anti-Rabbit,

Vector Labs, Inc., Burlingame, CA) for 60 min, followed by avidin conjugation (Vectastain Elite ABC Reagent, Vector Labs, Inc., Burlingame, CA) for 30 min at room temperature. Finally, staining was completed with 5–10 min incubation with diaminobenzidine (ImmPACT DAB Peroxidase, Vector Labs, Inc., Burlingame, CA). Slides were counterstained with hematoxylin, dehydrated and cover slipped.

Whole wound biopsies from all timepoints were scanned with a slide scanner (AxioScan.Z1, Carl Zeiss, Inc, Thornwood, NY) at 10 × magnification. Measurement of burn depth was performed with analysis software (ImagePro v6.2, Media Cybernetics, Inc., Rockville, MD). For each trichrome-stained image, 5 evenly spaced portions in the burned part of the biopsy were measured for total depth and averaged burned depth in terms of collagen coagulation. For caspase 3 analysis, the deepest edge of the apoptotic line was measured and divided into total dermal thickness to define burn depth. Analysis of HMGB1 was performed similar to a previous study utilizing the cellular location of HMGB1 which is normally nuclear [27]. Briefly, the deepest cytoplasmic localization of HMGB1 was measured and divided into total dermal thickness to calculate necrotic depth.”

2.7. Statistical analysis

Statistical evaluations were performed using analysis software (Prism, GraphPad Software Inc., San Diego, CA). Burn depth was analyzed with repeated measures 1 way ANOVA. SFDI and LSI were analyzed with 2-way ANOVA, with Bonferroni post hoc testing to examine contact time and days after-burn. For examining the abilities of non-invasive metrics to detect burn depth, linear regression analysis was performed. P values less than 0.05 were considered significant in all cases. Unless otherwise stated, all results are expressed as the arithmetic mean ± SEM.

3. Results

3.1. Animal recovery and wound appearance

No systemic effects were seen after thermal injury as the total %TBSA was ∼1.2% (area of 3 cm diameter probe × 16 wounds/ TBSA for 50 kg female swine) [39]. Representative photographs of wounds with progressively increasing contact times and areas of biopsy collection are shown in Fig. 1. All wounds have a pronounced zone of hyperemia (red edges) indicating a definitive burn wound border. Burn wounds with a short contact time (i.e. 5–10 s) are superficial second degree burn wounds, and have areas of red appearance within the wound. Burn wounds that have intermediate contact time (i.e. 15–25 s) are deep partial thickness in nature (still 2nd degree) and appear characteristically pale white. Wounds that are of longer contact duration (i.e. 35 s) are full thickness and appear necrotic by the end of the study.

3.2. Non-invasive imaging

3.2.1. SFDI—Representative images and analysis of SFDI across days and contact times for both the scattering coefficient (μ_s') (Fig. 2A) and oxygen saturation (Fig. 2B) are shown. Statistical analysis revealed a significant reduction in both of these parameters with increasing contact time, but no further changes were observed for the duration of the

experiment. The μ_s' for adjacent, unburned (normal) skin is 1.14 ± 0.041, with a coefficient of variation of 0.036. This parameter decreased for superficial burns with 5 s of contact time producing μ_s' of 1.563 ± 0.077 and 1.385 ± 0.063 at days 0 and 3, respectively. On the other hand, this decreased for full thickness burns as 40 s of contact time led to values of 0.984 ± 0.017 and 0.973 ± 0.06 at days 0 and 3, respectively. Oxygen saturation for normal skin is 55.4 ± 4.06%, with a coefficient of variation of 0.073, while for 5 s of contact time was 43.675 ± 5.732% and 45.2 ± 4.798% at days 0 and 3, respectively, and for 40 s of contact time it was 34.375 ± 5.782% and 22.90 ± 5.413% at days 0 and 3, respectively.

3.2.2. LSI—Representative images of LSI across days and contact times and analysis of blood flow using SFI measurements are shown in Fig. 2C. Lighter blue regions represent higher SFI values and greater blood flow, while darker regions represent reduced blood flow. Statistical analysis revealed a significant reduction in blood flow with increasing contact times, which continues to decrease for the duration of the experiment. The SFI value for normal skin is 923.0 ± 17.2, while for 5 s of contact time was 517.25 ± 10.09 and 482.25 ± 24.036 at days 0 and 4, respectively, and for 40 s of contact time it was 437.5 ± 7.67 and 393.0 ± 21.60 at days 0 and 4, respectively. The coefficient of variation for LSI-blood flow determined with an optical phantom was 0.014 (4.65/333.7).

3.3. Histological measurements of burn depth

3.3.1. Masson's trichrome—Changes in collagen coagulation due to increased contact times was determined histologically using Masson's trichrome stain [26]. Fig. 3A shows representative images for each contact time, and illustrates that with increasing contact times there is deeper collagen denaturation/coagulation. Fig. 3B quantifies this relationship on day 1 after-burn, with a regression of $y = 0.021x + 0.10$, and an r^2 of 0.84. Depth of collagen coagulation on day 1 was slightly deeper than what is seen on day 0 ($y = 0.018x - 0.06$, $r^2 = 0.72$). However, consistent with the mechanism of burn progression, there were no further changes in collagen coagulation on day 2 ($y = 0.021x + 0.11$, $r^2 = 0.89$) or day 3 ($y = 0.019x + 0.13$, $r^2 = 0.78$) (data not shown). The highest contact time of 40 s produced an almost complete coagulation of collagen in the dermis, with an average of 86 ± 4% of the dermis showing coagulation on day 1. Most importantly, the non-invasive SFDI-derived μ_s' correlated with the collagen coagulation determined histologically ($r^2 = 0.61$, Fig. 3C).

3.3.2. Apoptosis—Immunohistochemical detection of caspase 3 was performed to examine the relationship of apoptotic activation and noninvasive imaging. Caspase 3 is a protease implicated in the initiation of cell apoptosis, which has recently been shown to be sensitive in measuring burn depth as early as day 1 after-burn [28]. Fig. 4A shows representative images of caspase 3 expression and illustrates a distinct line of apoptosis, which penetrates deeper into the dermis with increasing contact times. Graph 4B demonstrates a linear regression which correlates this relationship, with a regression of $y = 1.41x + 53.94$, and an r^2 of 0.55. The highest contact time of 40 s produced apoptotic death through 100% of the dermis, and an additional 15.8% into the hypodermis (i.e. an average of 115.8 ±8% of dermal thickness) on day 1. Most importantly SFDI-derived μ_s' correlated with the apoptosis depth seen via caspase 3 staining ($r^2 = 0.28$) as shown in Fig. 4C.

3.3.3. Vascular/adnexal necrosis—Immunohistochemical detection of HMGB1, damage associated molecular pattern molecule, was performed to examine the necrotic aspect of burn depth on the day of burn. Previously this stain has been shown to detect adnexal and vascular necrosis between 1 and 24 h after-burn [28]. Fig. 5A shows representative images for each contact time, and demonstrates that HMGB1 is expressed outside of the nucleus adjacent to skin appendages/adnexae (e.g. hair follicles) and blood vessels in the dermis. Graph 5B demonstrates a linear regression which correlates this relationship on day 1 after burn with a regression of $y = 0.019 + 0.22$, and an $r2$ of 0.83. The highest contact time of 40 s produced necrosis throughout the dermis, with an average of 92.2 ± 5% of the dermis showing necrosis on day 1. Most importantly, LSI blood flow maps on day 0 correlated with the depth of necrosis seen via HMGB1 staining ($r^2 = 0.43$) as shown in Fig. 5C. Moreover, despite the reductions in LSI blood flow maps across days mentioned above, SFI values taken on day 4 continue to correlate with necrotic depth seen on the day of burn ($r^2 = 0.40$).

3.3.4. Burn heterogeneity—Heterogeneity in tissue damage in experimentally created burns in porcine models has been noted previously [29,31,40]. To further expand upon the relationship of scattering coefficients seen with collagen coagulation (Fig. 3) we examined the heterogeneity in biopsy strips which spanned the entire wound bed. Fig. 6 shows one example of a Masson's trichrome stained wound bed on day 4. While this burn wound was created with 40 s of contact time, and therefore very deep, there is an area of blue-stained collagen showing less severe coagulation. When juxtaposed to the associated spatial map of the SFDI-derived μ_s' parameter for that wound, the potential of this technology becomes apparent. The arrows point out that deeper coagulation corresponds to lower μ_s' values, which is consistent with the regression analysis seen in Fig. 3C ($y = 1.45x - 0.7$, $r^2 = 0.61$). Fig. 6C shows a picture of this wound, with the more pale appearance in the center represented by higher μ_s' values.

4. Discussion

Since the breakthrough concept was introduced by Dr. Janzekovic in the late 1970s, early excision and grafting has become the clinical standard for treatment of full and deep partial thickness burns [41,42]. Central to this strategy is debridement as early as possible after-burn to prevent infection and reduce scarring [43,44]. Currently, diagnosis of burn severity is performed visually and deep partial thickness burns are the most difficult to diagnose, even for an experienced burn surgeon [5,6,45]. This is especially true within the first 48 h where visual assessment has been shown to have an accuracy of less than 50% [8]. To aid in early diagnosis, a variety of non-invasive methods have been investigated for their ability to accurately assess burn depth, however none have become commonplace due various reasons such as resolution, cost, and long acquisition times [5,12]. Due to this, histopathology remains the most accurate way to determine burn severity, and collagen denaturation has been traditionally used to define depth of injury [26]. However, a recent study suggests that other histological approaches may be more sensitive than collagen denaturation, and may also give insight into burn depth earlier [28]. For example, necrosis and apoptosis have been shown to give insight into burn severity on the day of burn, which may correlate to non-

invasive imaging modalities. As such, we examined two promising imaging methods that render physiologically relevant parameters for their potential in predicting different aspects of burn depth.

Burns are complex wounds, with a number of physiological processes dictating severity [46]. While burn progression involving the zone of stasis results in spreading damage, the central zone of coagulation due to heat per se does not progress across days. This is reflected in our histological analysis as linear regression of collagen coagulation and contact times on day 1 after-burn (Fig. 3) were very similar to those seen on days 2 and 3 after-burn. Because of this, the reduced scattering coefficient (μ_s') generated from SFDI negatively correlated with collagen coagulation not only on day 1 after-burn, but also through the first 3 days after-burn. The μ_s' parameter is based off of the interactions of light with small particles and can be affected by the orientation and coagulation of those particles (i.e., dermal collagen). Moreover, using previously established formulas [47], the wavelengths used in this study (658–850 nm) have a calculated penetration depth of 0.8–2.2 mm. Additional wavelengths that accurately reflect changes in water concentration can also be incorporated with SFDI instrumentation. While not obvious in the current study, this would be able to incorporate any influence of swelling on derived parameters. The influence of connective tissue density/coagulation and the appropriate penetration depth lends μ_s' to be a good indicator of collagen denaturation.

The active form of caspase-3, a marker of apoptosis, has recently been shown to be expressed in the dermis after burn [28]. Similarly, in the current study we show that on day 1 after-burn there is a well-defined line of apoptotic cells illustrating burn depth (Fig. 4) and that increasing contact times positively correlate with depth of caspase-3 expression. Moreover, caspase 3 activation is also predicted with the SFDI derived μ_s' parameter. In addition, the SFDI-derived oxygenated hemoglobin (which is linked to measured chromophores) also correlates with apoptotic cell death, ($r^2 = 0.13$, $P = 0.04$, data not shown). This finding is interesting as we hypothesized that cell death (i.e. apoptotic depth) would be directly related to available oxygen in the dermis. Therefore, the assumption was that caspase-3 expression would be predicted more accurately by the physiologically-relevant oxygenated hemoglobin (calculated via chromophores) as opposed to scattering coefficients (calculated via structural properties). While that is not the case in the current model, oxygen saturation may have implications for burn healing at later time points. Regardless, SFDI appears to be able to noninvasively track certain important aspects of burn depth.

LDI has arguably progressed more than any other noninvasive technique in the clinic because of its accuracy improvement over visual assessment alone, although LDI is not as effective in the first 48 h [48]. LSI has a faster acquisition time and, in this study, we show that blood flow determined by LSI on day 0 and day 4 correlated with the damage associated molecular protein, high mobility group box 1 (HMGB1). Recently, Hirth et al. [27] showed that endothelial cell necrosis illustrated by HMGB1 taken 1 h after-burn is highly predictive of tissue necrosis 7 days after-burn. This data indicates a strong possibility that early use of LSI can predict burn progression in the several days following thermal injury.

Burn heterogeneity is routinely encountered in the clinic and is a motivating factor which highlights the importance of developing technology that noninvasively provides spatially resolved information over a wide-field view. Heterogeneity of burn wounds has been well-documented previously in porcine models [29,40]. We were able to overcome some of this heterogeneity by taking imaging measurements specifically where each biopsy was harvested. However, to address the spatial resolution of these technologies, we identified an example of this heterogeneity in biopsy strips spanning the entire wound bed taken on day 4 (Fig. 6). The associated spatial map of SFDI-derived μ_s' was then positioned next to that histological sample. The relationship with burn depth illustrated in Fig. 3C is reaffirmed. A reduction in μ_s' by ~25% of baseline levels (~1.2) was seen in areas of deep dermal collagen coagulation. While this only represents one sample, the baseline levels and their magnitude of change is consistent with Fig. 3C, and with previously studied values [22].

While 4 days after-burn may be ideal for diagnostic purposes, the advantage of other stains used in this study has been shown to be on the order of hours after-burn. Consistent with previous studies, expression of caspase 3 and HMGB1 in this study was limited to day 1 and immediately after-burn, respectively, and was not obvious on other days. This does, however, address the time range in which noninvasive imaging would be beneficial. While only 3 histological stains were used in this study, other groups have shown that these markers/stains are the most sensitive at determining different aspects of burn depth [28]. For example, polarized light was explored in the current study, but did not reveal any advantages over trichrome in determining the depth of collagen coagulation.

It is likely that one single parameter (e.g. blood flow) will not be sufficient for determining burn depth diagnostically, as other groups have indicated [5,49]. Most likely an algorithm that incorporates multiple non-invasive modalities will be able to monitor different aspects of burn depth for diagnostic purposes. Importantly, the assessment algorithm must have the spatial and temporal resolution to be able to “read” burn depth in real time, and over a sufficient region of interest. Taken together, the data presented here support a role for SFDI and LSI in non-invasively diagnosing several aspects of burn severity, which can be incorporated into such an algorithm.

Acknowledgments

The authors would like to thank the USAISR Veterinary Staff for their technical assistance with surgeries. Medical Research and Materiel Command (MRMC) provided funding for this project. Additional support is provided by the National Institutes of Health/NIBIB funded LAMMP (P41EB015890), the Military Medical Photonics Program (FA9550-10-1-0538), and the Arnold and Mabel Beckman Foundation.

References

1. Gibran NS, Wiechman S, Meyer W, Edelman L, Fauerbach J, Gibbons L, et al. American Burn Association consensus statements. J Burn Care Res. 2013; 34:361–85. [PubMed: 23835626]
2. Chan RK, Aden J, Wu J, Hale RG, Renz EM, Wolf SE. Operative utilization following severe combat-related burns. J Burn Care Res. 2014
3. Miller SF, Bessey P, Lentz CW, Jeng JC, Schurr M, Browning S, et al. National burn repository 2007 report: a synopsis of the 2007 call for data. J Burn Care Res. 2008; 29:862–70. discussion 71. [PubMed: 18997556]

4. H, D.; M, R.; E, L. Evaluation of the burn wound management decisions. In: Herndon, DN., editor. Total burn care. London: W.B Saunders; 2002. p. 101-8.
5. Devgan L, Bhat S, Aylward S, Spence RJ. Modalities for the assessment of burn wound depth. J Burns Wounds. 2006; 5:e2. [PubMed: 16921415]
6. McGill DJ, Sorensen K, MacKay IR, Taggart I, Watson SB. Assessment of burn depth: a prospective, blinded comparison of laser Doppler imaging and videomicroscopy. Burns. 2007; 33:833–42. [PubMed: 17614206]
7. Watts AM, Tyler MP, Perry ME, Roberts AH, McGrouther DA. Burn depth and its histological measurement. Burns. 2001; 27:154–60. [PubMed: 11226654]
8. Hoeksema H, Van de Sijpe K, Tondu T, Hamdi M, Van Landuyt K, Blondeel P, et al. Accuracy of early burn depth assessment by laser Doppler imaging on different days post burn. Burns. 2009; 35:36–45. [PubMed: 18952377]
9. Davis SC, Mertz PM, Bilevich ED, Cazzaniga AL, Eaglstein WH. Early debridement of second-degree burn wounds enhances the rate of epithelization – an animal model to evaluate burn wound therapies. J Burn Care Rehabil. 1996; 17:558–61. [PubMed: 8951545]
10. Eski M, Ozer F, Firat C, Alhan D, Arslan N, Senturk T, et al. Cerium nitrate treatment prevents progressive tissue necrosis in the zone of stasis following burn. Burns. 2012; 38:283–9. [PubMed: 22015201]
11. Firat C, Samdanci E, Erbatur S, Aytekin AH, Ak M, Turtay MG, et al. beta-Glucan treatment prevents progressive burn ischaemia in the zone of stasis and improves burn healing: an experimental study in rats. Burns. 2013; 39:105–12. [PubMed: 22469518]
12. Kaiser M, Yafi A, Cinat M, Choi B, Durkin AJ. Noninvasive assessment of burn wound severity using optical technology: a review of current and future modalities. Burns. 2011; 37:377–86. [PubMed: 21185123]
13. Arbab MH, Dickey TC, Winebrenner DP, Chen A, Klein MB, Mourad PD. Terahertz reflectometry of burn wounds in a rat model. Biomed Opt Express. 2011; 2:2339–47. [PubMed: 21833370]
14. Cross KM, Leonardi L, Gomez M, Freisen JR, Levasseur MA, Schattka BJ, et al. Noninvasive measurement of edema in partial thickness burn wounds. J Burn Care Res. 2009; 30:807–17. [PubMed: 19692905]
15. Cross KM, Leonardi L, Payette JR, Gomez M, Levasseur MA, Schattka BJ, et al. Clinical utilization of near-infrared spectroscopy devices for burn depth assessment. Wound Repair Regen. 2007; 15:332–40. [PubMed: 17537120]
16. Sowa MG, Leonardi L, Payette JR, Cross KM, Gomez M, Fish JS. Classification of burn injuries using near-infrared spectroscopy. J Biomed Opt. 2006; 11:054002. [PubMed: 17092151]
17. Sowa MG, Leonardi L, Payette JR, Fish JS, Mantsch HH. Near infrared spectroscopic assessment of hemodynamic changes in the early post-burn period. Burns. 2001; 27:241–9. [PubMed: 11311517]
18. Benya R, Quintana J, Brundage B. Adverse reactions to indocyanine green: a case report and a review of the literature. Cathet Cardiovasc Diagn. 1989; 17:231–3. [PubMed: 2670244]
19. Pape SA, Skouras CA, Byrne PO. An audit of the use of laser Doppler imaging (LDI) in the assessment of burns of intermediate depth. Burns. 2001; 27:233–9. [PubMed: 11311516]
20. Stewart CJ, Frank R, Forrester KR, Tulip J, Lindsay R, Bray RC. A comparison of two laser-based methods for determination of burn scar perfusion: laser Doppler versus laser speckle imaging. Burns. 2005; 31:744–52. [PubMed: 16129229]
21. Gioux S, Mazhar A, Cuccia DJ, Durkin AJ, Tromberg BJ, Frangioni JV. Three-dimensional surface profile intensity correction for spatially modulated imaging. J Biomed Opt. 2009; 14:034045. [PubMed: 19566337]
22. Mazhar A, Sharif SA, Cuccia JD, Nelson JS, Kelly KM, Durkin AJ. Spatial frequency domain imaging of port wine stain biochemical composition in response to laser therapy: a pilot study. Lasers Surg Med. 2012; 44:611–21. [PubMed: 22911574]
23. Pharaon MR, Scholz T, Bogdanoff S, Cuccia D, Durkin AJ, Hoyt DB, et al. Early detection of complete vascular occlusion in a pedicle flap model using quantitative [corrected] spectral imaging. Plast Reconstr Surg. 2010; 126:1924–35. [PubMed: 21124132]

24. Yafi A, Vetter TS, Scholz T, Patel S, Saager RB, Cuccia DJ, et al. Postoperative quantitative assessment of reconstructive tissue status in a cutaneous flap model using spatial frequency domain imaging. Plast Reconstr Surg. 2011; 127:117–30. [PubMed: 21200206]
25. Nguyen JQ, Crouzet C, Mai T, Riola K, Uchitel D, Liaw LH, et al. Spatial frequency domain imaging of burn wounds in a preclinical model of graded burn severity. J Biomed Opt. 2013; 18:66010. [PubMed: 23764696]
26. Chvapil M, Speer DP, Owen JA, Chvapil TA. Identification of the depth of burn injury by collagen stainability. Plast Reconstr Surg. 1984; 73:438–41. [PubMed: 6199804]
27. Hirth D, McClain SA, Singer AJ, Clark RA. Endothelial necrosis at 1 hour postburn predicts progression of tissue injury. Wound Repair Regen. 2013; 21:563–70. [PubMed: 23627744]
28. Hirth DA, Singer AJ, Clark RA, McClain SA. Histopathologic staining of low temperature cutaneous burns: comparing biomarkers of epithelial and vascular injury reveals utility of HMGB1 and hematoxylin phloxine saffron. Wound Repair Regen. 2012; 20:918–27. [PubMed: 23126459]
29. Singer AJ, McClain SA. A porcine burn model. Methods Mol Med. 2003; 78:107–19. [PubMed: 12825265]
30. Sullivan TP, Eaglstein WH, Davis SC, Mertz P. The pig as a model for human wound healing. Wound Repair Regen. 2001; 9:66–76. [PubMed: 11350644]
31. Gaines C, Poranki D, Du W, Clark RA, Van Dyke M. Development of a porcine deep partial thickness burn model. Burns. 2013; 39:311–9. [PubMed: 22981797]
32. Cuccia DJ, Bevilacqua F, Durkin AJ, Ayers FR, Tromberg BJ. Quantitation and mapping of tissue optical properties using modulated imaging. J Biomed Opt. 2009; 14:024012. [PubMed: 19405742]
33. Ponticorvo A, Taydas E, Mazhar A, Scholz T, Kim HS, Rimler J, et al. Quantitative assessment of partial vascular occlusions in a swine pedicle flap model using spatial frequency domain imaging. Biomed Opt Express. 2013; 4:298–306. [PubMed: 23412357]
34. Mazhar A, Dell S, Cuccia DJ, Gioux S, Durkin AJ, Frangioni JV, et al. Wavelength optimization for rapid chromophore mapping using spatial frequency domain imaging. J Biomed Opt. 2010; 15:061716. [PubMed: 21198164]
35. Erickson TA, Mazhar A, Cuccia D, Durkin AJ, Tunnell JW. Lookup-table method for imaging optical properties with structured illumination beyond the diffusion theory regime. J Biomed Opt. 2010; 15:036013. [PubMed: 20615015]
36. Aguilar G, Choi B, Broekgaarden M, Yang O, Yang B, Ghasri P, et al. An overview of three promising mechanical, optical, and biochemical engineering approaches to improve selective photothermolysis of refractory port wine stains. Ann Biomed Eng. 2012; 40:486–506. [PubMed: 22016324]
37. Yang O, Cuccia D, Choi B. Real-time blood flow visualization using the graphics processing unit. J Biomed Opt. 2011; 16:016009. [PubMed: 21280915]
38. Choi B, Ramirez-San-Juan JC, Lotfi J, Stuart Nelson J. Linear response range characterization and in vivo application of laser speckle imaging of blood flow dynamics. J Biomed Opt. 2006; 11:041129. [PubMed: 16965157]
39. Kelley KW, Curtis SE, Marzan GT, Karara HM, Anderson CR. Body surface area of female swine. J Anim Sci. 1973; 36:927–30. [PubMed: 4703721]
40. Kempf M, Cuttle L, Liu PY, Wang XQ, Kimble RM. Important improvements to porcine skin burn models, in search of the perfect burn. Burns. 2009; 35:454–5. [PubMed: 18947931]
41. Janzekovic Z. A new concept in the early excision and immediate grafting of burns. J Trauma. 1970; 10:1103–8. [PubMed: 4921723]
42. Orgill DP. Excision and skin grafting of thermal burns. N Engl J Med. 2009; 360:893–901. [PubMed: 19246361]
43. Cramer LM, Mc CR, Carroll DB. Progressive partial excision and early graftin in lethal burns. Plast Reconstr Surg Transplant Bull. 1962; 30:595–9. [PubMed: 14023665]
44. Engrav LH, Heimbach DM, Reus JL, Harnar TJ, Marvin JA. Early excision and grafting vs nonoperative treatment of burns of indeterminant depth: a randomized prospective study. J Trauma. 1983; 23:1001–4. [PubMed: 6355500]

45. Hop MJ, Moues CM, Bogomolova K, Nieuwenhuis MK, Oen IM, Middelkoop E, et al. Photographic assessment of burn size and depth: reliability and validity. J Wound Care. 2014; 23:144–5. 8–52. [PubMed: 24633060]

46. Shupp JW, Nasabzadeh TJ, Rosenthal DS, Jordan MH, Fidler P, Jeng JC. A review of the local pathophysiologic bases of burn wound progression. J Burn Care Res. 2010; 31:849–73. [PubMed: 21105319]

47. Cuccia DJ, Bevilacqua F, Durkin AJ, Tromberg BJ. Modulated imaging: quantitative analysis and tomography of turbid media in the spatial-frequency domain. Opt Lett. 2005; 30:1354–6. [PubMed: 15981531]

48. Jaskille AD, Ramella-Roman JC, Shupp JW, Jordan MH, Jeng JC. Critical review of burn depth assessment techniques: part II. Review of laser Doppler technology. J Burn Care Res. 2010; 31:151–7. [PubMed: 20061851]

49. Ganapathy P, Tamminedi T, Qin Y, Nanney L, Cardwell N, Pollins A, et al. Dual-imaging system for burn depth diagnosis. Burns. 2014; 40:67–81. [PubMed: 23790396]

Abbreviations

SFDI	spatial frequency domain imaging
LSI	laser speckle imaging
LDI	laser Doppler imaging

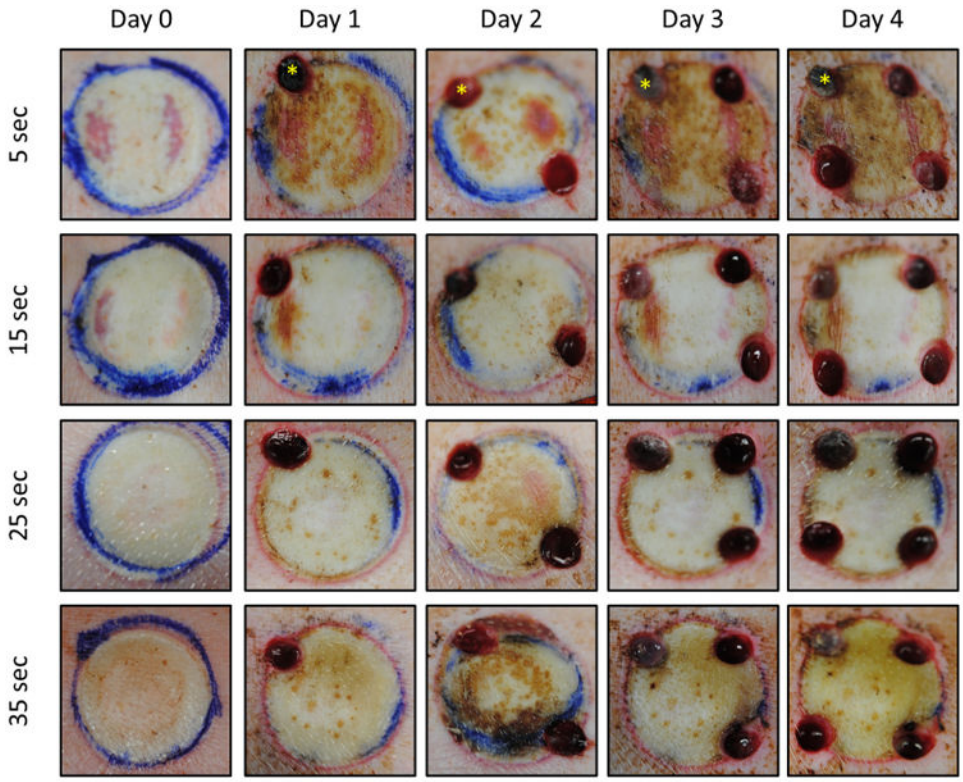

Fig. 1.

Gross morphology of burn wounds. Photographs of burn wounds with increasing contact time over the timecourse of the experiment. Burn wounds of 5 s show areas of very superficial depth as seen with the mottled, pink appearance which is evident through the dried blood on days 3 and 4. Burn wounds of 15 and 25 s both have characteristic deep partial appearance, with a pale center. Burn wounds of 35 s appear yellowish, consistent with full thickness burn. All wounds present with a prominent zone of stasis. The day 0 biopsy in the 5 s wound is denoted with an asterisk, and biopsy punches from the subsequent days are apparent at the edges of the wound.

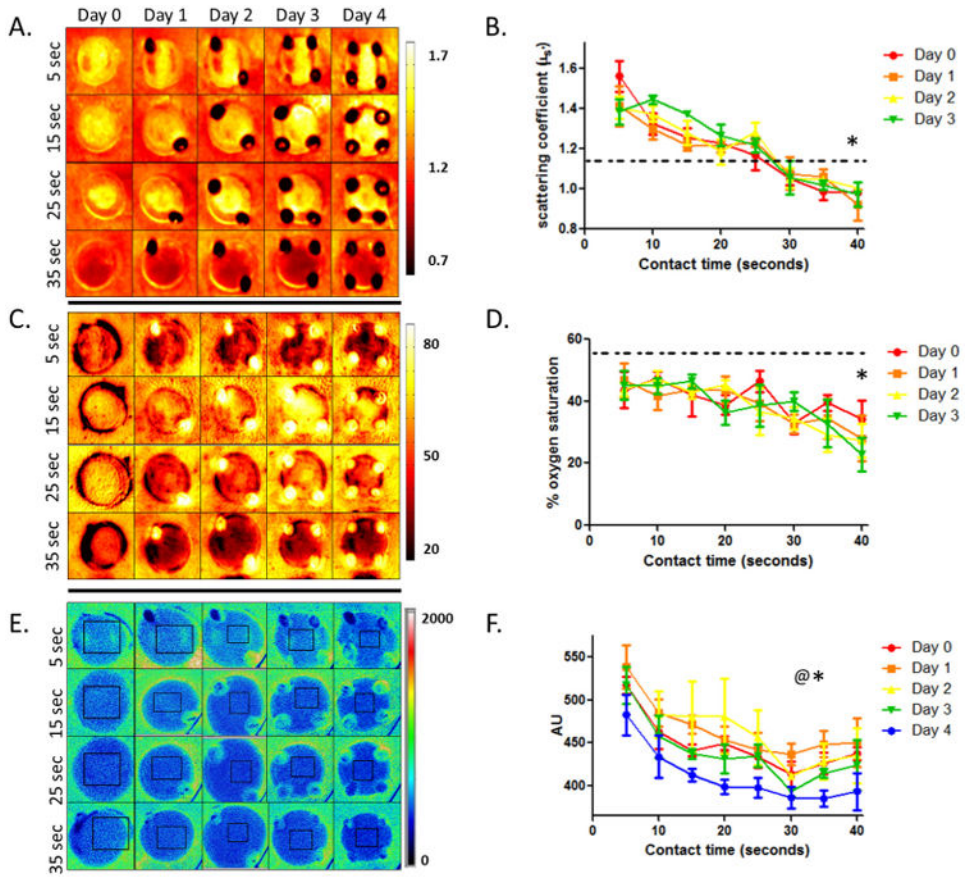

Fig. 2.

Differences in non-invasive imaging metrics versus contact times for each day after-burn. Left panels show representative images and scales for SFDI-derived scattering coefficients (μ_s') (A) and oxygen saturation (C), and LSI-derived blood flow (E). The right panels show μ_s' (B) and oxygen saturation (D), and LSI-derived blood flow (F) plotted against contact time (n = 4 burns/contact time). 2-Way ANOVA reveals a significant effect of contact time for μ_s', oxygen saturation, and blood flow (* $P < 0.001$, $P = 0.0153$, and $P < 0.0001$, respectively). Additionally, there is a significant change in blood flow due to time, with a reduction out to day 4 after-burn (@ $P < 0.0001$). Dotted lines reveal normal (unburned) values for μ_s' and oxygen saturation, while normal blood flow values were drastically higher (923.0 ± 17.2).

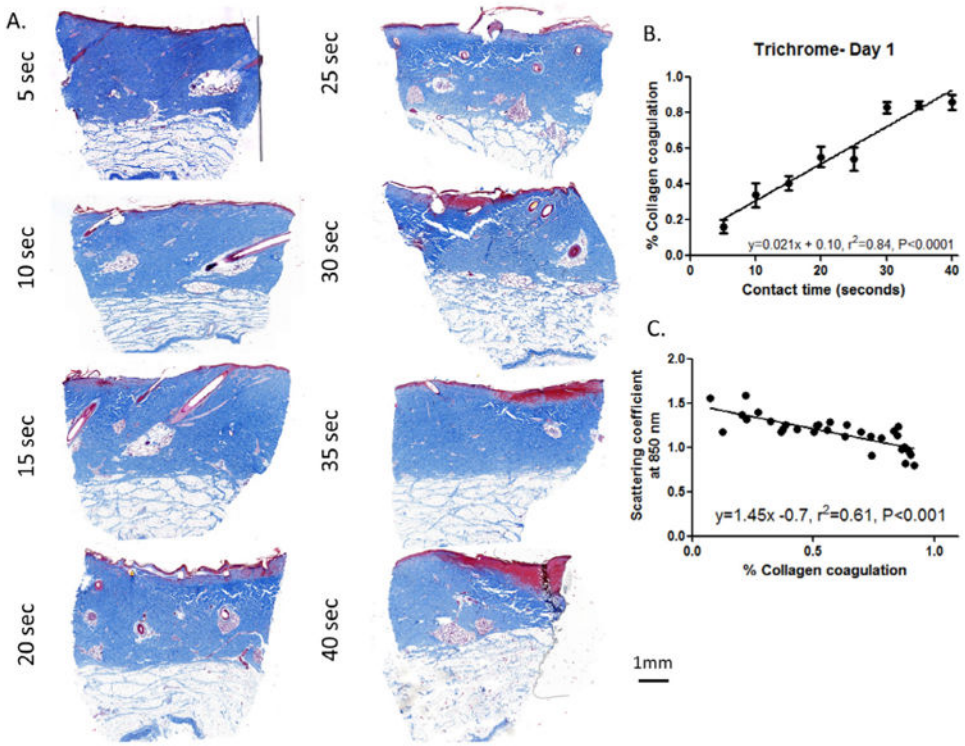

Fig. 3.

Trichrome staining of collagen coagulation following burn and non-invasive imaging with SFDI. (A) Representative images and (B) linear regression analysis of trichrome stained biopsies reveals longer contact times lead to deeper collagen coagulation 1 day after-burn, $r^2 = 0.84$, $P < 0.001$. (C) Non-invasive imaging with SFDI reveals a significant correlation with μ_s' and depth of collagen coagulation 1 day after-burn, $r^2 = 0.61$, $P < 0.001$.

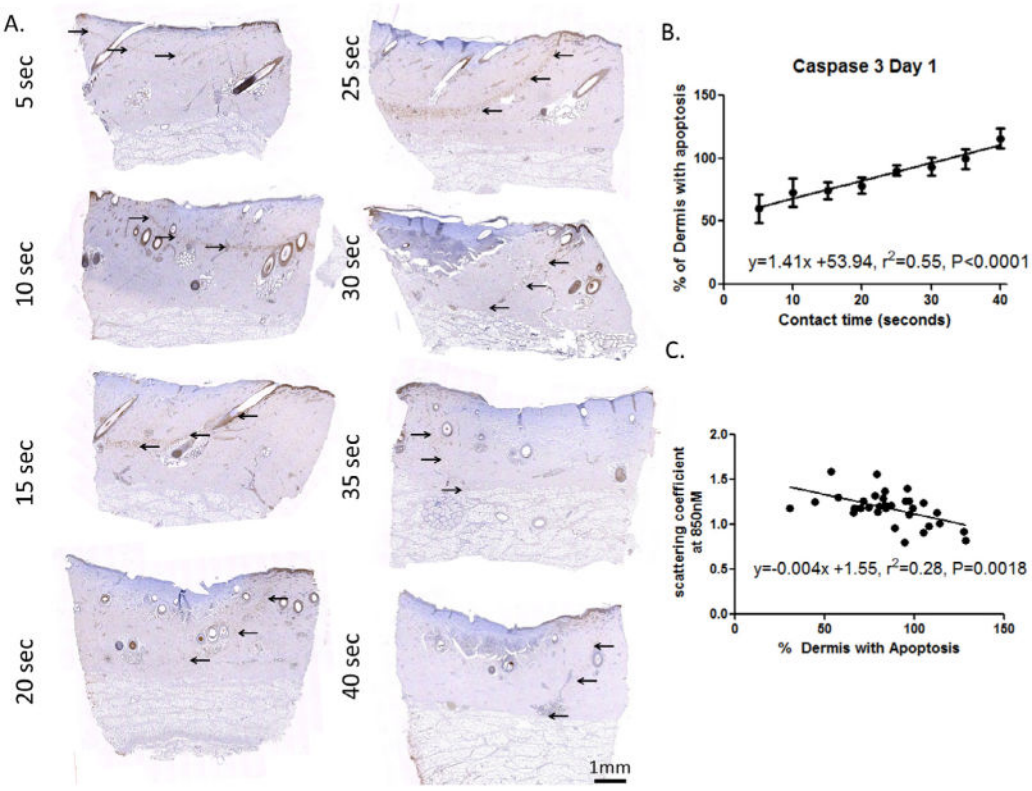

Fig. 4.

Depth of caspase 3 expression following burn is correlated with SFDI. (A) Representative images of immunostaining for caspase 3 reveals a line of apoptotic cells (arrows) 1 day after-burn that becomes deeper with increasing contact times as shown in the linear regression analysis. (B) Longer duration of probe contact time leads to a deeper line of apoptosis, $r^2 = 0.55$, $P < 0.0001$. (C) The μ_s' measured non-invasively with SFDI reveals a significant correlation with depth of apoptosis 1 day after-burn, $r^2 = 0.28$, $P = 0.0018$.

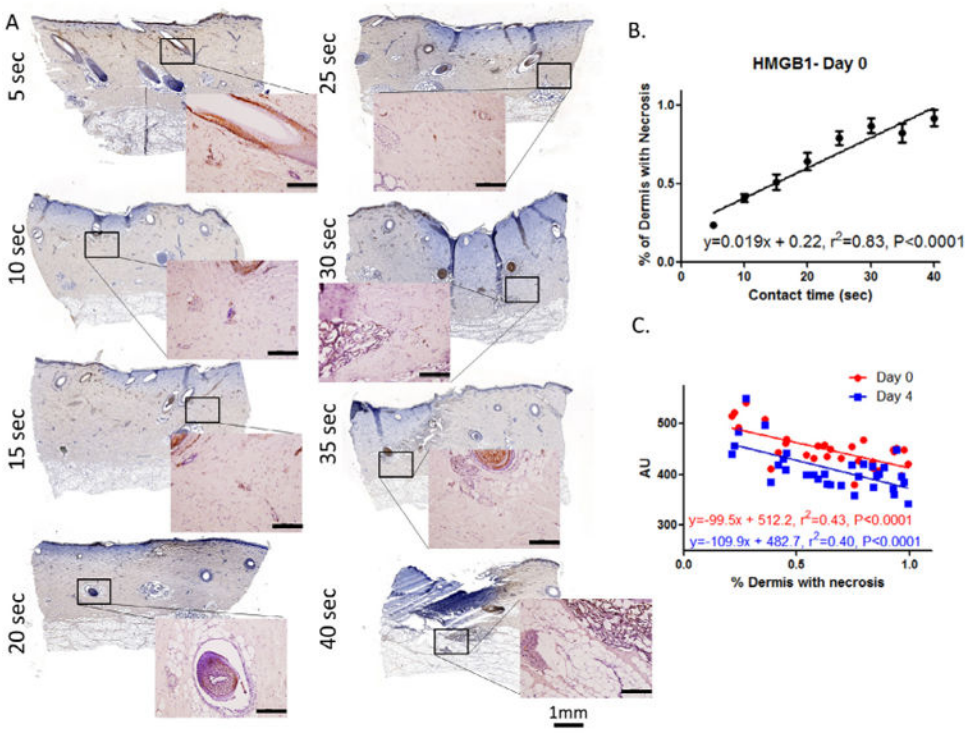

Fig. 5.

Vascular and adnexal necrosis is correlated with LSI. (A) Representative images of immunostaining for HMGB1 reveals adnexal and vascular necrosis on day 0 that becomes deeper with increasing contact times as shown in the linear regression analysis. Scale bar for the higher magnification images is 200 μm. (B). Longer duration of probe contact time leads to a greater depth of necrosis, $r^2 = 0.83$, $P < 0.0001$. (C) Blood flow measured non-invasively with LSI reveals a significant correlation with depth of necrosis on the day of thermal injury. This relationship holds true with laser speckle imaging on both day 0 ($r^2 = 0.43$) and day 4 after-burn ($r^2 = 0.40$).

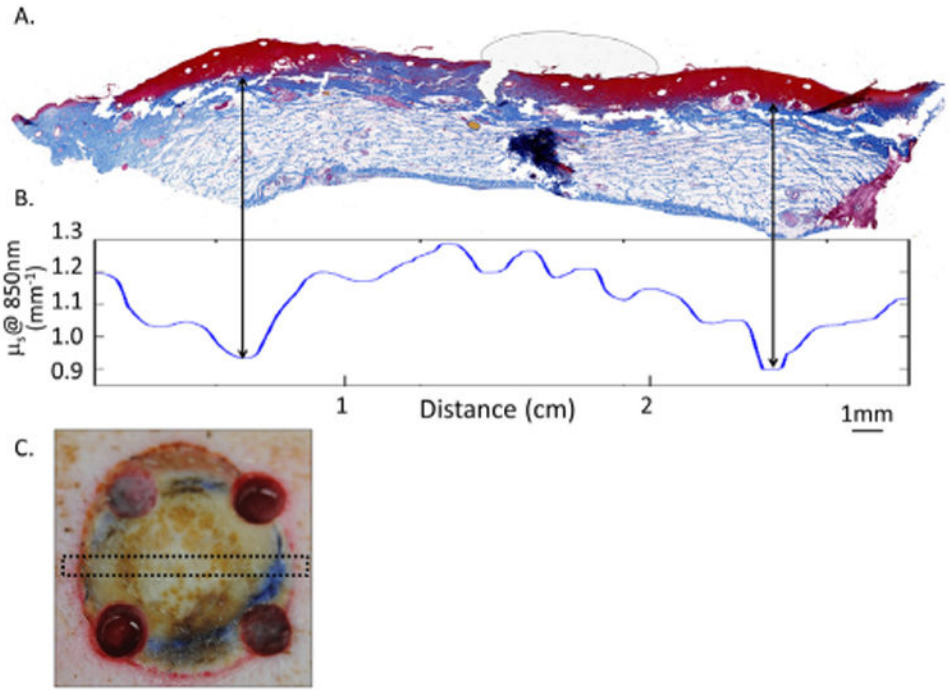

Fig. 6.

SFDI detects burn wound heterogeneity on day 4. Burn depth heterogeneity on a strip biopsy from day 4 (A), and μ_s' plots over the complete wound bed for the same sample are shown (B). Similar to that seen in Fig. 2, reductions in the μ_s' readouts correspond to deeper burn depth. Picture in (C) shows the same wound with an approximate location of the biopsy indicated with dashed lines.